Structure of an RNA Hairpin Loop with a 5′-CGUUUCG-3′ Loop Motif by Heteronuclear NMR Spectroscopy and Distance Geometry[†]

Christian Sich, Oliver Ohlenschläger, Ramadurai Ramachandran, Matthias Görlach, and Larry R. Brown*

Institut für Molekulare Biotechnologie eV, Abteilung für Molekulare Biophysik/NMR Spektroskopie, Postfach 100 813, D-07708 Jena, Germany

Received May 22, 1997; Revised Manuscript Received August 18, 1997[⊗]

ABSTRACT: Structural features of a 19-nucleotide RNA hairpin loop (5′-GGCGUACGUUUCGUACGCC-3′), a loop motif which occurs in eukaryotic 18S rRNA, have been derived using multidimensional heteronuclear NMR spectroscopy in combination with local conformational analysis and torsion angle distance geometry followed by restrained energy minimization. A method to obtain both the $^3J_{C4'P3'}$ and $^3J_{C4'P5'}$ coupling constants from a set of spin-echo difference constant time HSQC spectra is introduced, and it is shown how these couplings can be assigned to the backbone angles β and ϵ. A total of 280 distance constraints as well as 132 homo- and heteronuclear three-bond scalar coupling constants were derived from the NMR data. The structure which has been determined is a pentaloop rather than a triloop with no base pairing between G8 and C12. G8 is pointed to the minor groove where it forms a base triplet with C7-G13 that is further stabilized by hydrogen bonding to the 2′-hydroxyl group of C7. C12 is directed to the major groove where its conformation is stabilized by hydrogen bonding between O2 and HO2′. The NMR data suggest two possible, interconverting conformations with stacking of bases U10-G8 or U11-C7. Overall, the loop provides a variety of interaction sites for RNA or protein interactions.

Besides its role in information transfer, RNA is associated with regulatory functions or catalytic activity, with these functions carried out either by the RNA alone or in conjunction with associated proteins. Unfortunately, three-dimensional structural information obtained for RNA is limited so far. X-ray diffraction techniques require ordered crystals of adequate size, which has so far been possible for tRNAs and small RNA fragments as well as recently for the hammerhead ribozyme (Pley et al., 1994b; Scott et al., 1996) and the group I ribozyme domain (Cate et al., 1996). The structures of small secondary structural motifs such as hairpin loops, bulges, internal loops, or pseudoknots have been obtained by solution NMR[1] spectroscopy [for reviews see, e.g., Moore (1993), Shen et al. (1995), and Feigon et al. (1996)]. The size of the RNA molecules studied by NMR has recently been extended to approximately 40 nucleotides by the introduction of isotope labeling (Wyatt et al., 1991; Nikonowicz et al., 1992; Batey et al., 1992) and the development of NMR experiments appropriate for isotope-labeled RNA molecules (Dieckmann & Feigon, 1994; Pardi, 1995; Moore, 1995; Varani et al., 1996).

Hairpin loops are among the most abundant structural elements in RNA. They provide nucleation sites for RNA folding (Uhlenbeck, 1990; Woese et al., 1990), occur at transcription termination sites, provide sites for interaction with proteins, and can be involved in stabilization of RNA tertiary structure (Cate et al., 1996). The traditional view of RNA hairpins in which the stem was considered to be highly structured and the loop disordered is contradicted by many hairpin structures solved recently (Cheong et al., 1990; Heus & Pardi, 1991b; Varani et al., 1991; Puglisi et al., 1990; Hoffman et al., 1993; Mirmira & Tinoco, 1996; Fountain et al., 1996; Szewczak et al., 1993; Laing & Hall, 1996; Orita et al., 1993; Pley et al., 1994a). Although some hairpin loops have conformational flexibility (Jaeger & Tinoco, 1993; Colvin et al., 1993), such loops can take up a distinct structure by interaction with either a protein, as has been shown for internal loops (Aboul-ela et al., 1995; Allain et al., 1996), or an RNA molecule (Gregorian & Crothers, 1995; Marino et al., 1995a).

In the hairpin structures of 16S-like rRNAs investigated by Wolters (1992), tetraloops are preferred to 60% in bacteria but to a much lesser degree (46%) in eukaryotes. Triloops occur less frequently but are still quite common; e.g., the UUU family is found in 3% of the tight loops in 16S rRNA in bacteria and in about 12% of these in eukaryotes, mainly with the loop sequences UUU and UCU. The most abundant triloop sequence, UUU, combines preferentially with CU_AG as nearest neighbors in bacteria and with CG_CG in eukaryotes. In the latter, the number of continuous base pairs adjacent to the loop exceeds four. As investigated by Woese et al. (1990) in bacterial 16S rRNA, the hairpin loop at position 83 (*Escherichia coli* numbering) occurs mainly as a tetraloop, but additionally the triloop UUU sequence has arisen independently several times.

With the advent of isotope $^{13}C/^{15}N$-labeled RNA and the recent advances in NMR spectroscopy, we decided to try to obtain a detailed structure of a hairpin loop with a 5′-CGUUUCG-3′ loop motif, in which the UUU loop is in the context of CG_CG. This sequence motif occurs frequently in ribosomal RNA (Wolters, 1992), and a very similar loop

---

[†] This work has been supported by Deutsche Forschungsgemeinschaft Grant Br 1487/1 and by the Fonds der Chemischen Industrie.

[⊗] Abstract published in *Advance ACS Abstracts,* October 15, 1997.

[1] Abbreviations: COSY, correlated spectroscopy; CT-HSQC, constant time heteronuclear single-quantum coherence; E.COSY, exclusive COSY; NMP, nucleoside 5′-monophosphate; NMR, nuclear magnetic resonance; NOE, nuclear Overhauser effect; NOESY, NOE spectroscopy; NTP, nucleoside 5′-triphosphate; TOCSY, total correlation spectroscopy; WATERGATE, water suppression by gradient-tailored excitation; 11-mer, 5′-GGCGUUUCGCC-3′; 15-mer, 5′-GGCACGUUUCGUGCC-3′; 19-mer, 5′-GGCGUACGUUUCGUACGCC-3′.

(5′-GGUCUCC-3′) forms the E-loop of *E. coli* 5S rRNA (nt 85−91). In addition, medium resolution structures of 5′-UU(UCU)GA-3′ (Puglisi et al., 1990) and 5′-GC(UUU)-GC-3′ (Davis et al., 1993) triloop motifs have previously been obtained by hydrogen and phosphorus NMR. The large number of scalar coupling constants and NOEs which could be determined using heteronuclear ^{15}N- and ^{13}C-edited NMR data, together with 3D structure determination by local conformational analysis and distance geometry with subsequent energy minimization, indicated that the 5′-CGUUUCG-3′ loop motif adopts a pentaloop conformation differing from all previously studied triloop hairpin molecules.

MATERIALS AND METHODS

Sample Preparation. Three RNA oligonucleotides, 5′-GGCGUUUCGCC-3′ (referred to as 11-mer), 5′-GGCACG-UUUCGUGCC-3′ (15-mer), and 5′-GGCGUACGUUUC-GUACGCC-3′ (19-mer), were prepared by *in vitro* transcription with T7 RNA polymerase from synthetic DNA templates with a double-stranded promotor region (Milligan et al., 1987). DNA oligonucleotides were synthesized using phosphoramidite chemistry. Prior to transcription the promotor strand was annealed to the template strand by heating 5 μM template strand, 5 μM promotor strand, 6 mM $MgCl_2$, 1 mM spermidine, and 40 mM Tris-HCl, pH 8.1, for 3 min at 95 °C and slowly cooling the mixture to room temperature. ^{15}N- and ^{15}N/^{13}C-labeled nucleotides were prepared by growth of *E. coli* strain MRE600 on M9 media containing [^{15}N] ammonium chloride (>98%, ISOTEC and Cambridge Isotope Laboratories) or [^{15}N] ammonium chloride/[^{13}C] glucose (99%, Cambridge Isotope Laboratories) as the sole nitrogen/carbon source, respectively. Subsequently ribosomes were isolated and rRNA extracted, followed by enzymatic digestion of the RNA to NMPs and phosphorylation to NTPs (Wyatt et al., 1991; Nikonowicz et al., 1992; Batey et al., 1992; Grüne et al., 1996b). Transcription reactions were incubated overnight at 37 °C [40 mM Tris-HCl pH 8.1, 1 mM spermidine, 80 mg/mL poly(ethylene glycol), 28 mM $MgCl_2$, 20 mM dithiothreitol, 600 nM DNA template, 4 mM each NTP, 0.1 mg/mL T7 RNA polymerase] using either ^{15}N- or ^{15}N/^{13}C-labeled NTPs. Afterward the solution was extracted with phenol/chloroform, and the nucleic acids were obtained by ethanol precipitation. The final ^{15}N-labeled 11-mer and 15-mer products were purified by reversed-phase ion pair chromatography (Pingoud et al., 1989) on a preparative Vydac protein and peptide C18 column equilibrated with 50 mM potassium phosphate and 2 mM tetrabutylammonium hydrogen sulfate, pH 5.9 in water. The RNA was eluted using an acetonitrile gradient. The collected product was lyophilized and the salt removed with a Centricon-3 microconcentrator (Amicon). Traces of tetrabutylammonium hydrogen sulfate were removed by subsequent precipitation of the RNA with 5 volumes of 2% lithium perchlorate in acetone. The ^{15}N- or ^{15}N/^{13}C-labeled 19-mer was purified by preparative acrylamide gel electrophoresis under denaturing conditions (7 M urea). The product was cut from the gel, electroeluted (Bio-Rad, Electro Eluter), and precipitated with ethanol. The final RNA products were dialyzed with a Centricon-3 microconcentrator first against 100 mM NaCl, 10 mM EDTA, 50 μM NaN_3, and 10 mM sodium phosphate, pH 6.0, to remove traces of divalent impurities (Puglisi & Tinoco, 1989) and second against the final NMR buffer containing 90% H_2O/10% D_2O, 5 μM EDTA, 50 μM NaN_3, 10 mM sodium phosphate, pH 6.0, and different concentrations of NaCl. Final yields (incorporation of nucleotides into the purified RNA) were approximately 3.5% for ^{15}N-labeled 11-mer, 2.5% for ^{15}N-labeled 15-mer, 2% for ^{15}N-labeled 19-mer, and 1.5% for ^{15}N/^{13}C-labeled 19-mer. A D_2O sample of the ^{15}N/^{13}C-labeled RNA 19-mer was prepared by lyophilizing the sample three times from 99.9% D_2O. The lyophilized material was then dissolved in 99.995% D_2O. The final concentration of the ^{15}N/^{13}C-labeled 19-mer was 0.5 mM.

NMR Spectroscopy. NMR experiments were performed on Varian 600 UnityPlus or 750 INOVA spectrometers. One- and two-dimensional experiments were processed with the program VNMR (Varian). Three-dimensional experiments were processed with the program PROSA (Güntert et al., 1992) on Sun or Silicon Graphics workstations. Subsequently, two- and three-dimensional spectra were analyzed using the program XEASY (Bartels et al., 1995). The multidimensional NMR experiments which were acquired are given in the text, and the details of the acquisition and processing parameters are given in Table 1 in the Supporting Information.

Distance Restraints. Upper limit distance constraints for the nonexchangeable hydrogens were calculated from NOE cross peak volumes using the isolated spin pair approximation with the program CALIBA (Güntert et al., 1991). Averaged cytosine and uracil H5−H6 cross peak volumes of stem nucleotides were taken as references with a fixed distance of 2.42 Å for the 2D (^{1}H, ^{1}H) NOESY spectrum (Kumar et al., 1980) and the 3D (^{13}C, ^{1}H, ^{1}H) NOESY spectrum (Norwood et al., 1990) of the aromatic region. The ribose-optimized 3D (^{13}C, ^{1}H, ^{1}H) NOESY spectrum was calibrated using H1′−H2′ cross peaks of the stem nucleotides (C3′-endo ribose conformation) with a reference distance of 2.8 Å. Mixing times of 80 and 100 ms were used for 2D and 3D experiments, respectively, to minimize spin diffusion effects. The relaxation delay was 6 s for the 2D experiment, corresponding to approximately $3T_1$ as measured from standard inversion recovery experiments. A relaxation delay of 6 s is prohibitively long for a 3D experiment. We therefore used only 2.5 s, which is slightly longer than the longitudinal relaxation time of the slowest relaxing hydrogens. The influences of the relaxation delay and of the relative calibration of the three spectra were examined by comparing the scaled volumes for cross peaks which could be measured in all the different spectra. The deviation of cross peak volumes in the different spectra to the mean value varied from about ±20% for strong cross peaks to ±80% for the weakest cross peaks, which is the order of magnitude expected for error margins of intensities between differently processed spectra obtained for close mixing times (Schmitz & James, 1995). The average volumes were taken for the conversion of cross peak volumes to distance constraints with the program CALIBA (Güntert et al., 1991). For the input to the DIANA structure calculations, the usual pseudoatom corrections for nonstereospecifically assigned hydrogens were applied (Güntert et al., 1991). NOEs involving exchangeable hydrogens observed in the 200 ms NOESY experiment in H_2O were interpreted more conservatively. Strong and weak cross peaks were given upper bounds of 5 and 7 Å, respectively. No lower limits were used for the NOE-derived distance constraints (Varani et al., 1996). Hydrogen-bonding constraints were introduced for the base pairs G2−C18 to

C7−G13, for which the NH and NH_2 resonances fulfilled the criteria described by Allain and Varani (1995). These were introduced as upper limits between heavy atoms of 3 Å and an additional lower limit constraint of 9.1 Å between N1 and N9 atoms of the two bases involved in the hydrogen bonding.

Scalar Coupling Constants. 2D (^{13}C, ^{1}H) HCCH-E.COSY, 3D (^{1}H, ^{13}C, ^{1}H) HCCH-E.COSY, and 3D (^{1}H, ^{13}C, ^{1}H) "directed" HCC-TOCSY-CCH-E.COSY experiments (Griesinger & Eggenberger, 1992; Olsen et al., 1993; Schwalbe et al., 1994; Schwalbe et al., 1995; Marino et al., 1996) were acquired, and the $^{3}J_{HH}$ coupling constants were measured as displacements of the multiplet components in the direct dimension, neglecting the small contributions of the nonconnected transitions. To account for this, the scalar coupling constants were given an error margin of at least ±1 Hz. To restrict the backbone torsion angles β and ϵ, heteronuclear $^{3}J_{PH}$ and $^{3}J_{CP}$ coupling constants were measured. A standard 2D (^{13}C, ^{1}H) HSQC experiment (Bodenhausen & Ruben, 1980) without phosphorus decoupling provided $^{3}J_{H3'P}$, $^{3}J_{H5'P}$, and $^{3}J_{H5''P}$ coupling constants via the typical E.COSY pattern due to the associated $^{2}J_{CP}$ couplings (Schmieder et al., 1992). The additional $^{1}J_{CC}$ couplings observed in the present experiment were not removed by using constant time experiments (Santoro & King, 1992; Vuister & Bax, 1992) due to the limited sensitivity at long indirect acquisition times.

$^{3}J_{C2'P}$ and $^{3}J_{C4'P}$ are associated with small four-bond scalar couplings and are themselves small in the case of $^{3}J_{C2'P}$ or show couplings to two phosphorus atoms simultaneously ($^{3}J_{C4'P}$ except for the 3′-terminal residue). To determine $^{3}J_{C2'P}$ and $^{3}J_{C4'P}$ a set of spin-echo difference 2D (^{13}C, ^{1}H) CT-HSQC spectra (Vuister et al., 1993) with constant times of $1/J_{CC}$, $2/J_{CC}$, and $3/J_{CC}$ were analyzed. For $^{3}J_{C2'P}$ the relative difference in signal volumes of the H2′C2′ cross peaks between ^{31}P-decoupled and ^{31}P-coupled spectra was employed to derive scalar coupling constants as described by Legault et al. (1995). The H2′C2′ cross peak of C19 was used to evaluate the minimal errors for the relative signal volumes. The H4′C4′ cross peak volumes are influenced by two passive scalar couplings in the ^{31}P-coupled spectra versus the ^{31}P-decoupled spectra because C4′ is coupled to the 5′ phosphorus as well as the 3′ phosphorus via three bonds. The relative cross peak volumes are $V_{coup}/V_{decoup} = \cos(\pi\,^{3}J_{C4'P3'}CT)\cos(\pi^{3}J_{C4'P5'}CT)$, where V_{coup} and V_{decoup} are the cross peak volumes in the ^{31}P-coupled and decoupled spectra, respectively, and CT is the constant time used. The experimental ratio of V_{coup}/V_{decoup} corresponds to an allowed area on a $^{3}J_{C4'P3'}$, $^{3}J_{C4'P5'}$ hyperplane which depends on the constant time. The intersection of all allowed areas provides the possible values of $^{3}J_{C4'P3'}$ and $^{3}J_{C4'P5'}$. To determine which of the two $^{3}J_{C4'P}$ coupling constants is to the 3′ and 5′ phosphorus, respectively, we recorded a standard 3D HCP experiment (Heus et al., 1994) in which the signal intensity of the H4′C4′P peak is dependent on the size of the C4′P scalar coupling. By qualitatively comparing the cross peak intensities of the peaks to the 5′ phosphorus and 3′ phosphorus, the $^{3}J_{C4'P}$ coupling constants could be ascribed to the torsion angle β or ϵ. Systematic errors in the determination of these coupling constants with spin-echo difference CT-HSQC experiments could arise from improper inversion of the ^{31}P 180° pulse and be due to faster relaxation of antiphase ^{13}C magnetization compared to in-phase ^{13}C magnetization (Vuister et al., 1993). We accounted for this by increasing by ±1 Hz the possible range of the scalar coupling constants determined as described above.

Dihedral Angle Constraints. Scalar coupling constants and NOE distance constraints were translated into dihedral angle restraints by local conformational analysis (Ohlenschläger, unpublished results; see acknowledgment). In short, a grid search which varied the angles β, γ, δ, ν_1, ν_2, χ, and ϵ with 10° step size was performed over all possible conformations of a mononucleotide. Scalar coupling constants were translated into dihedral angle restraints using Karplus curves from Altona (1982) for $^{3}J_{H1'H2'}$ and $^{3}J_{H2'H3'}$, from Altona and Sundaralingam (1973) for $^{3}J_{H3'H4'}$ and $^{3}J_{H4'H5'/H5''}$, from Lee and Sarma (1976) for $^{3}J_{PH5'/H5''}$, from Mooren et al. (1994) for $^{3}J_{H3'P}$, and from Plavec and Chattopadhyaya (1995) for $^{3}J_{C2'P}$ and $^{3}J_{C4'P}$. For each conformation a target function similar to the one used in the program DIANA (Güntert et al., 1991) was evaluated. NOE, van der Waals, and dihedral angle violations contributed to this target function. Conformations which had target functions below a threshold of 0.01−0.2 Å^2 were stored. The region containing all dihedral angles which were found in the accepted conformations was used as the dihedral angle restraint in the subsequent distance geometry structure calculation. This procedure also gave stereospecific assignments for some of the H5′H5″ hydrogens. For residues in which the 5′ hydrogens were not stereospecifically assigned, the dihedral angle constraints include the dihedral angle ranges obtained for each of the possible stereospecific assignments. Additionally, the α and ζ angles were restrained (to 0 ± 120°) to exclude the trans conformation if the ^{31}P chemical shift of the involved phosphorus did not show large downfield shifts (Gorenstein, 1984; Varani et al., 1991).

Structure Calculation and Analysis. The input for the first distance geometry calculations with the program DIANA (Güntert et al., 1991) consisted of NOE derived upper limits, hydrogen-bonding constraints, constraints for the ribose ring to obtain proper ribose geometries, and dihedral angle constraints derived from the local conformational analysis of scalar coupling constants and intranucleotide NOEs as described above. Several rounds of structure calculations and NOESY cross peak assignments using the program ASNO (Güntert et al., 1993) were performed. After structure calculation with the full data set, close hydrogen−hydrogen contacts in the loop region which were not defined by restraints were found. We therefore checked all hydrogen−hydrogen distances smaller than 3 Å in a set of 20 structures for the existence of cross peaks in the NOE spectra. If no cross peak was found, this distance was introduced as a "non-NOE" (Schmitz & James, 1995) distance restraint with a lower bound of 3 Å. In total, 38 lower limit constraints were introduced for residues C7−G13. In the final round of the DIANA structure calculation, all measured upper distance limits, lower distance limits for the loop region, the dihedral angle constraints mentioned above, and stereospecific assignments obtained for some of the stem nucleotides from the local conformational analysis process were used. Starting with 300 randomized conformers, five REDAC cycles (Güntert & Wüthrich, 1991) were performed in which the maximal target function value per residue for locally acceptable segments was set to $T_{local}^{(1-3)} = 0.6$ Å^2 and $T_{local}^{(4,5)} = 0.4$ Å^2, for minimizations 2−4 and 5,6, respectively. At least 30 structures with acceptable local target functions were required in order for the observed torsion angles to be included as angle constraints in subsequent REDAC cycles. In the final cycle only the experimentally measured dihedral angle constraints were used.

The 15 DIANA conformers with the smallest target function values were subjected to restrained energy minimization using the program AMBER 4.1 (Pearlman et al., 1995) with the AMBER all-atom force field (Cornell et al., 1995). A flat-bottomed potential for a fulfilled distance limit/dihedral angle range and subsequent parabolic curvature up to 0.5 Å or 10° above the limit followed by a linear increase was used for both distance and dihedral restraints with force constants of 25 kcal/(mol Å^2) and 50 kcal/(mol rad^2), respectively. A distance-dependent dielectric constant of $\epsilon = r$ was employed. The negative charges on the phosphate groups were reduced to -0.2, and no explicit counterions were used. Nonbonded interactions were cut off at 12 Å. Steepest descent minimization was performed until the difference in the norm of the gradient for successive steps was within 0.1 kcal/(mol Å) followed by conjugate gradient minimization until a 0.05 kcal/(mol Å) difference. To represent the solution structure of the RNA 19-mer, the resulting 15 energy-refined structures were used. Structures were analyzed using the programs XAM (Xia, 1992) and MOLMOL (Koradi et al., 1996). The latter program was also used to generate figures showing the structures and torsion angles.

RESULTS

Preparation of Monomeric Stem–Loop Structures. Due to the self-complementarity of the stem sequence, small hairpin loops may alternatively form duplex structures. Initial NMR observations of the imino hydrogen region for the 11-mer indicated formation of three UU base pairs (Figure 1A and unpublished results), which suggested that this loop motif can alternatively form a duplex structure with three consecutive UU base pairs. Although imino hydrogen resonances of the monomeric species can also be observed for the 11-mer as shown in Figure 1A, it was not possible to find conditions with sufficiently high RNA concentration under which no duplex resonances were observed. Indeed, although the proportion of the monomeric stem–loop species in the NMR samples could be increased to as much as 90% by rapid quenching of the sample temperature from 90 to 0 °C, for the 11-mer rapid equilibration led to re-formation of the predominant dimeric species within about 0.5 h. Even the extension of the stem region by two base pairs was not sufficient to obtain exclusively the monomeric species as monitored by the characteristic sharp uridine imino resonances in the upfield imino region (15-mer, Figure 1B). For the 15-mer, the monomeric species obtained by rapid quenching of the sample temperature was observed to equilibrate to a substantial proportion of dimeric species within about 20 h. Only the introduction of two further stem base pairs was observed to result in pure hairpin conformation under conditions of 10 mM sodium phosphate buffer at pH 6.0 with RNA concentrations of up to 1.6 mM (19-mer, Figure 1C). For the 19-mer, following quenching from 90 °C, no formation of a dimeric species was observed over a period of several months. For all three different RNA molecules, the number of sharp imino hydrogen resonances observed in the NMR spectra of the monomeric stem loop was always two less than suggested by the number of potential Watson–Crick base pairs in the stem region (e.g., six sharp imino resonances and eight potential base pairs for the 19-mer; Figure 1C). Although fraying of the base pair at the end of the stem region commonly leads to the nonobservation of one imino hydrogen resonance for stem regions, the consistent nonobservation of two imino hydrogen resonances was a first indication that the 5′-CGUUUCG-3′ motif forms a pentaloop independent of stem lengths of ≥4 base pairs.

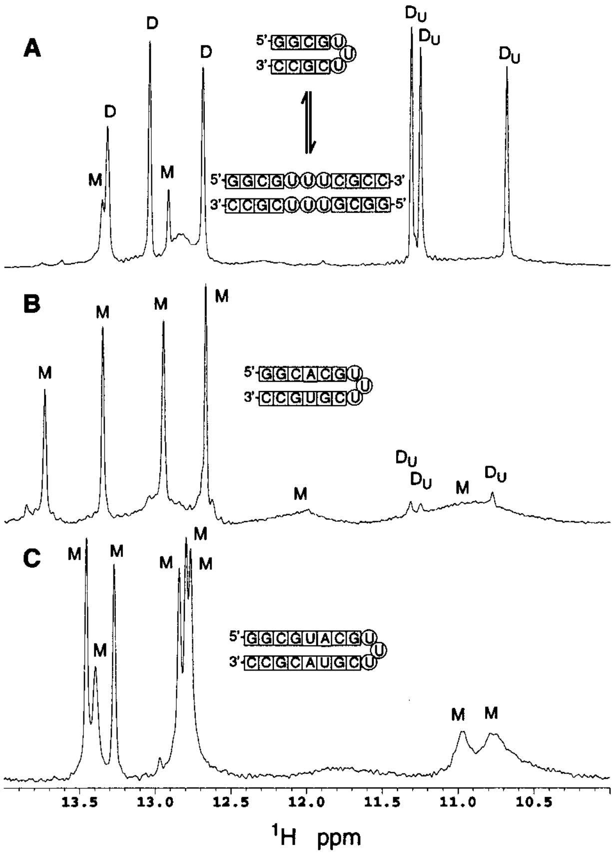

FIGURE 1: Imino region of one-dimensional ^{1}H NMR spectra of the (A) 11-mer, (B) 15-mer, and (C) 19-mer RNA molecules recorded in 90% H_2O/10% D_2O with binomial water suppression. Conditions are 10 mM phosphate, pH 6.0, 20 °C [except (C) at 30 °C], and RNA concentrations of 1.35, 0.6, and 1.6 mM for the 11-mer, 15-mer, and 19-mer, respectively. The sequences and secondary structure models for the three molecules are shown with each spectrum. In (A) resonances corresponding to monomer and dimer species are marked M and D, respectively. The uridine dimer resonances are marked D_U. The characteristic ^{15}N chemical shifts observed in 2D (^{15}N, ^{1}H) correlation spectra confirm the assignment for these uridine resonances (data not shown).

Resonance Assignments. Nonexchangeable hydrogen and carbon resonances of the RNA 19-mer were assigned in four steps: First, individual ribose spin systems were identified. Second, base hydrogen/carbon spin systems were determined. Third, base and ribose spin systems were linked. Fourth, nucleoside spin systems were mapped onto the sequence.

Ribose hydrogen and carbon spin systems have been identified by a strategy similar to that described by Nikonowicz and Pardi (1993). Hydrogens were linked to the attached carbon by standard 2D (^{13}C, ^{1}H) HSQC (Bodenhausen & Ruben, 1980) and constant time HSQC (Santoro & King, 1992; Vuister & Bax, 1992) experiments. By using chemical shift arguments (Varani & Tinoco, 1991) as well as the different number of carbon–carbon one-bond interactions, 1′, 2′/3′, 4′, and 5′ resonances can be distinguished.

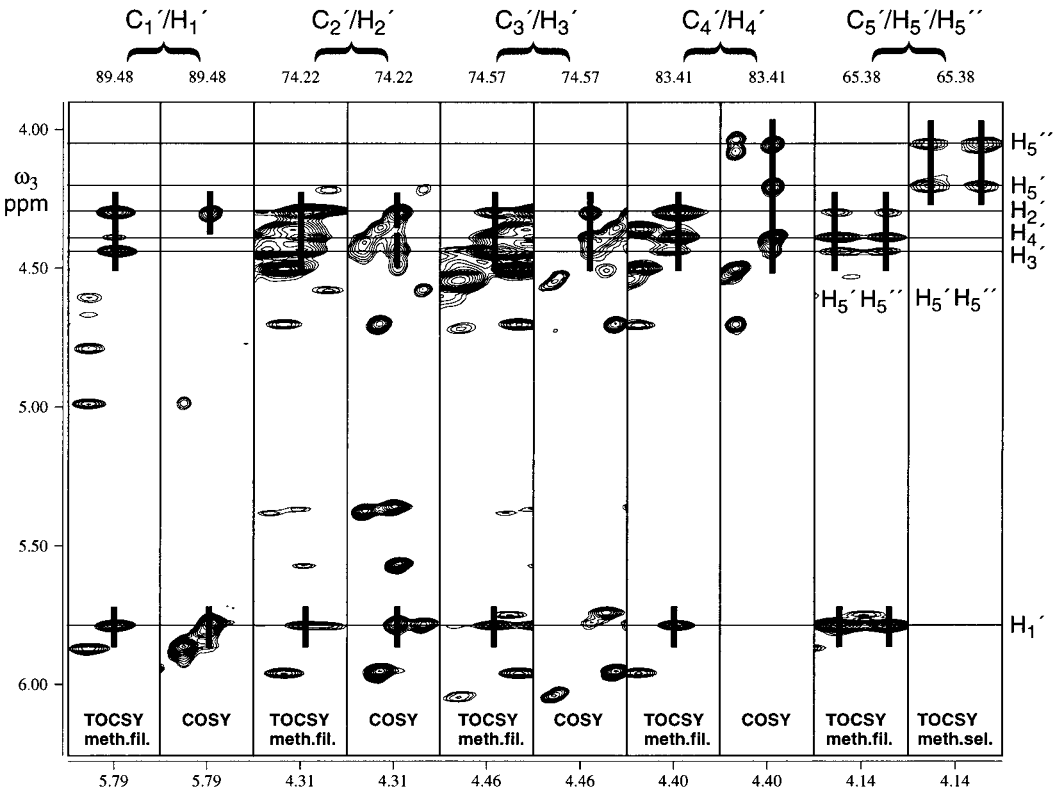

FIGURE 2: Identification of the ribose ring system of U9. Strips are taken at the ^{1}H, ^{13}C chemical shifts of each hydrogen−carbon pair in the ribose ring in methylene-filtered, methylene-selected 3D HCCH-TOCSY or 3D HCCH-COSY experiments. The shifts of the ribose ring hydrogens are marked by thin lines in the ω_3 dimension. The identified signals are marked by thick vertical lines. The chemical shift positions of the strips are given at the top of the strip for the carbon plane and at the bottom for the hydrogen position in the ω_1 dimension.

All 19 of the C1′H1′ cross peaks were individually resolved for this hairpin. The CH groups of individual ribose rings were linked using methylene-filtered/methylene-selected 3D HCCH-TOCSY and 3D HCCH-COSY experiments (Fesik et al., 1990; Kay et al., 1990; Bax et al., 1990; Clore et al., 1990; Pardi & Nikonowicz, 1992). A typical set of strips from methylene-filtered/methylene-selected 3D HCCH-TOCSY and 3D HCCH-COSY experiments is shown in Figure 2 for the ribose resonances of residue U9. Using these procedures all ribose hydrogen and carbon resonances for the 19-mer could be unambiguously assigned.

Base hydrogens were linked via a 2D HCCH-COSY experiment (Kay et al., 1990; Clore et al., 1990; Bax et al., 1990; Pardi & Nikonowicz, 1992) optimized for magnetization transfer between H5 and H6 in the case of pyrimidines and via a 2D HCCH-TOCSY experiment (Legault et al., 1994; Marino et al., 1994a) for the correlation of H2 and H8 hydrogens in adenosine. The attached carbon resonances could be determined from the (^{13}C, ^{1}H) HSQC experiment. Ribose and base spin systems were linked using a 2D (^{15}N, ^{1}H) HCN experiment (Sklenar et al., 1993). The experiment, which was carried out in a nonselective fashion, provided H1′ to aromatic hydrogen (H6 or H8) links for 14 out of the 19 residues.

Sequential assignments were obtained using two independent strategies. In the through-bond approach residues are linked via the intervening phosphorus resonance (Heus et al., 1994; Marino et al., 1994b, 1995b; Tate et al., 1995). Here we used a new experiment, HC(N/P)-CCH-TOCSY (Ramachandran et al., 1996), which provides valuable information on base types via the ^{15}N chemical shifts that can be used for the clarification of ambiguous sequential assignments in the HCP-CCH-TOCSY subspectrum. For a detailed description of this approach as applied to the 19-mer studied here, see Ramachandran et al. (1996). For the through-space approach via NOESY spectroscopy (Varani & Tinoco, 1991; Moore, 1995), a 400 ms 2D (^{1}H, ^{1}H) NOESY experiment (Kumar et al., 1980) as well as a 400 ms 2D (^{1}H, ^{1}H) purine/pyrimidine-selective NOESY experiment (Ramachandran et al., 1997) was recorded. The latter experiment provides NOE subspectra for NOEs arising from purine H8 and pyrimidine H6 hydrogens, respectively, thereby simplifying the sequential assignment procedure. For a detailed description of this approach applied to the present 19-mer, see Ramachandran et al. (1997).

The chemical shifts of the nonexchangeable hydrogens are given in Table 2 in the Supporting Information and the heteronuclear shifts in Table 3 in the Supporting Information. Some carbon resonances for residues G8, C12, G13, and U14 (Table 3, Supporting Information) were found to have broader line widths, particularly for carbons of the ribose rings, in the standard HSQC and other experiments. These broader resonances, which were found for residues at the boundary between the stem and loop, remained broad over the temperature range 5−27 °C. The broader line widths prevented the correlation of the U14 phosphorus resonance as well as the C12 and G13 N1/N9 base nitrogens to the attached carbons, therefore preventing the assignment of these resonances.

Exchangeable hydrogens were assigned on the basis of 2D (^{1}H, ^{1}H) WATERGATE-NOESY and 2D (^{15}N, ^{1}H) WATERGATE-HSQC experiments (Lippens et al., 1995; Grzesiek & Bax, 1993) at 5 °C. Imino and amino hydrogens generally resonate in distinct spectral regions (Wüthrich, 1986; Varani & Tinoco, 1991). The ^{15}N chemical shift of the attached nitrogen provides additional information due to

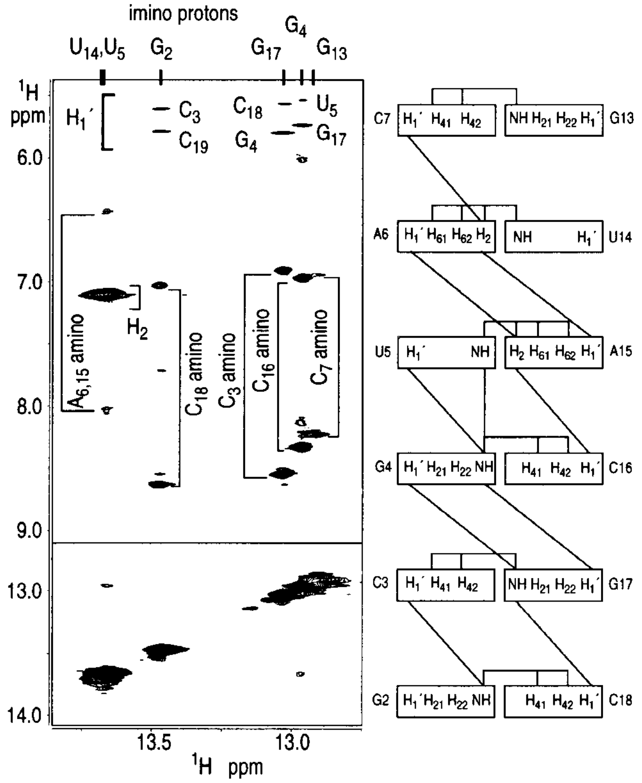

FIGURE 3: NOEs to imino hydrogens as observed in the 2D (^{1}H, ^{1}H) NOESY experiment in H_2O at 5 °C with a mixing time of 200 ms. In the right part of the figure NOEs to imino protons as well as H_2 protons are shown schematically for the helix region of the 19-mer.

the fact that guanosine and uridine imino nitrogens as well as cytosine, adenosine, and guanosine amino nitrogens tend to resonate in different spectral regions (Nikonowicz & Pardi, 1993). Therefore, exchangeable hydrogen resonances were tentatively assigned to hydrogen and base types from the 2D (^{15}N, ^{1}H) WATERGATE HSQC spectrum. Sequence-specific assignments were then obtained from the 2D (^{1}H, ^{1}H) WATERGATE NOESY experiment with a mixing time of 200 ms (see Figure 3) using standard procedures (Wüthrich, 1986; Varani & Tinoco, 1991; Nikonowicz & Pardi, 1993). NOE interactions between guanosine imino hydrogens and H1′ hydrogens as described by Heus and Pardi (1991a) were also used for assignment. The observed NOE connectivities provide clear sequential assignments and unambiguously establish Watson−Crick base pairing from base pairs G2−C18 to C7−G13 (Figure 3). The imino resonances of the loop uridines 9−11, which gave broad resonances near 10.5−11.0 ppm (Figure 1), could not be sequentially assigned due to the lack of observable NOEs as a consequence of fast exchange with solvent. For G1 and G8 no imino resonances and for C12 no amino resonances could be detected. No evidence for base pairing of G8 to C12 has been found. The assignments for the exchangeable hydrogens and their attached nitrogens are shown in Tables 2 and 3 in the Supporting Information, respectively.

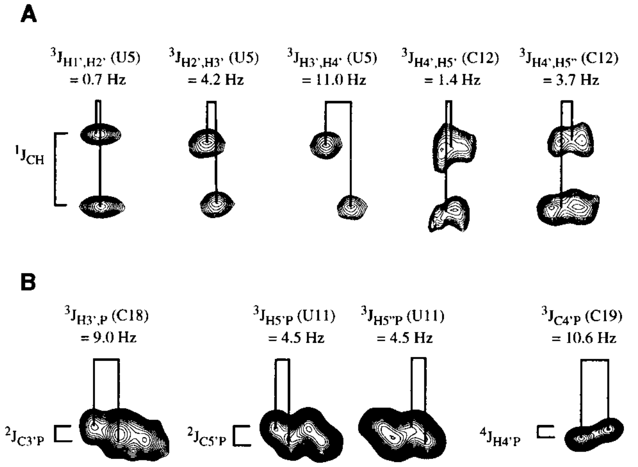

FIGURE 4: Determination of $^3J_{HH}$, $^3J_{HP}$, and $^3J_{CP}$ scalar couplings. (A) Typical cross peaks for the determination of the $^3J_{HH}$ couplings. The first cross peak is taken from the 2D HCCH-E.COSY, the next two are from the 3D HCCH-E.COSY, and the last two are from the 3D HCC-TOCSY-CCH-E.COSY experiment. The vertical dimension is the ^{13}C dimension, showing the large associated $^1J_{CH}$ coupling. The scalar couplings are measured in the final ^{1}H dimension. (B) Cross peaks from a standard HSQC experiment without phosphorus decoupling for the determination of $^3J_{HP}$ and $^3J_{CP}$ scalar couplings. Here the three-bond couplings are associated with smaller two- or four-bond couplings. Because other residues have two such couplings, $^3J_{C4'P}$ could only be determined for the 3′-terminal residue.

Coupling Constants. Homonuclear $^3J_{HH}$ coupling constants (Griesinger & Eggenberger, 1992; Olsen et al., 1993; Schwalbe et al., 1994, 1995; Marino et al., 1996), as well as $^3J_{PH}$ and $^3J_{CP}$ coupling constants (Bodenhausen & Ruben, 1980; Schmieder et al., 1992), were measured in the typical E.COSY patterns as displacements of the multiplet components in the direct dimension (Figure 4). About 70% of all possible $^3J_{HH}$ couplings and 60% of $^3J_{PH}$ and $^3J_{CP}$ coupling constants could be determined. The main reason for not obtaining a scalar coupling constant was overlap even in 3D spectra. This was especially a problem for H4′ to H5′/H5″ scalar couplings in the stem region due to the minimal dispersion of the C4′ chemical shifts for these resonances. Especially for residues C12 and G13, no or only very weak cross peaks could be observed, presumably as a consequence of the larger carbon line widths leading to magnetization losses during the ^{13}C−^{13}C COSY or TOCSY transfers.

$^3J_{C2'P}$ and $^3J_{C4'P}$ were measured from a set of spin-echo difference 2D (^{13}C, ^{1}H) CT-HSQC spectra (Vuister et al., 1993) acquired with constant times of $1/J_{CC}$, $2/J_{CC}$, and $3/J_{CC}$ and with and without ^{31}P decoupling (Legault et al., 1995). The H4′C4′ cross peak volumes are influenced by two passive scalar couplings in the ^{31}P-coupled spectra versus the ^{31}P-decoupled spectra because C4′ is coupled to the 5′ phosphorus as well as 3′ phosphorus via three bonds. The $^3J_{C4'P}$ couplings were extracted from theoretical plots (Figure 5) of $V_{coup}/V_{decoup} = \cos(\pi^3J_{C4'P3'}CT)\cos(\pi^3J_{C4'P5'}CT)$, where V_{coup}, and V_{decoup} are the cross peak volumes in the ^{31}P-coupled and -decoupled spectra, respectively, and CT is the constant time used. Using this new approach for the determination of $^3J_{C4'P}$ couplings, it was possible to measure 70 scalar coupling constants which defined β or ϵ.

Inter-Hydrogen Distances and Dihedral Constraints. Upper limit distance constraints were extracted from a 2D (^{1}H, ^{1}H) NOESY spectrum, a 3D (^{13}C, ^{1}H, ^{1}H) NOESY experiment optimized for the ribose region in the first two dimensions, and a 3D (^{13}C, ^{1}H, ^{1}H) NOESY experiment optimized for the aromatic region in the indirect dimensions as described in Materials and Methods. The intranucleotide NOEs and scalar coupling constants were converted into the dihedral angle constraints given in Table 6 in the Supporting Information by use of local conformational analysis (Ohlenschläger, unpublished results; see Acknowledgment). Due

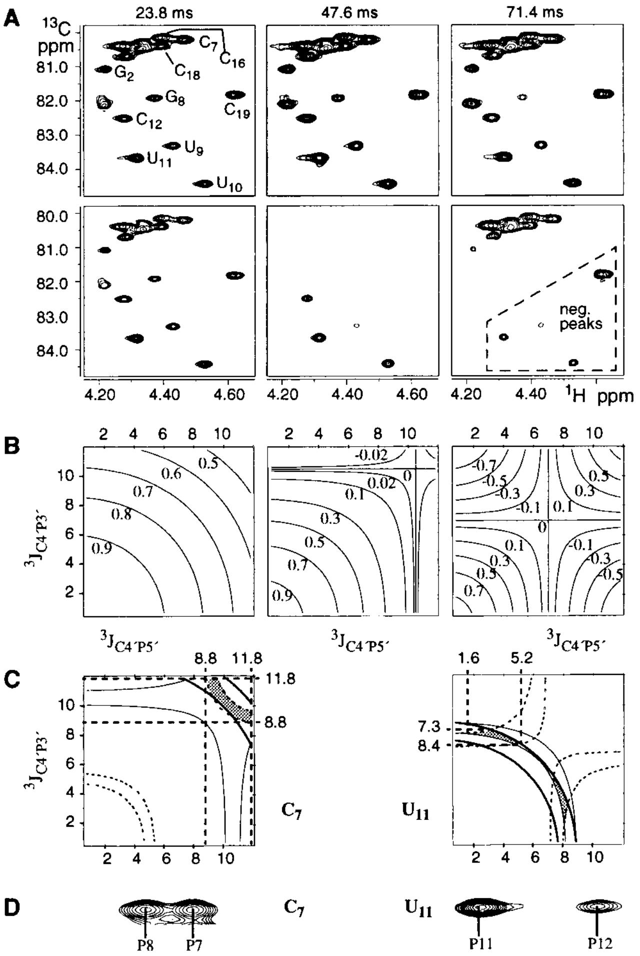

FIGURE 5: Determination of $^{3}J_{C4'P}$. (A) H4′C4′ regions of the spin-echo difference CT-HSQC spectra recorded at the constant times given above the spectra. The upper spectra were acquired without the phosphorus scalar coupling and the lower spectra with the passive scalar coupling of the C4′ to phosphorus during the constant time. The spectra are phased such that the spectra without the phosphorus coupling have positive H4′C4′ peaks. The spectra at one constant time are plotted at the same threshold. In the first spectrum the resonances for which the $^{3}J_{C4'P}$ couplings could be determined are marked by the residue type and number. (B) Contour plots of the relative peak volumes V_{coup}/V_{decoup} as a function of the two scalar coupling constants $^{3}J_{C4'P5'}$ and $^{3}J_{C4'P3'}$. The plots are calculated for 23.8 ms (left), 47.6 ms (middle), and 71.4 ms (right) constant time periods, respectively. (C) Determination of the two scalar coupling constants, $^{3}J_{C4'P5'}$ and $^{3}J_{C4'P3'}$ for C7 (left) and U11 (right). The thick lines border the allowed combinations of scalar coupling constants obtained from the 23.8 ms spin-echo difference spectra, the thin lines those obtained from the 47.6 ms spectra, and the dotted lines those from the 71.4 ms spectra, respectively. The intersections of the three areas are shaded and show the allowed combinations of the two coupling constants. The maximal ranges for each of the coupling constants are indicated by dashed lines. Note that the two coupling constants can be interchanged. (D) Cross peaks in the C_4' planes from a 3D HCP experiment shown for the same residues C7 and U11. The horizontal and vertical dimensions correspond to phosphorus and hydrogen frequencies, respectively. If $^{3}J_{C4'P5'}$ and $^{3}J_{C4'P3}$ have sufficiently different magnitudes (as for U11), the different intensities of the P,C4′,H4′ cross peaks can be used to specifically assign $^{3}J_{C4'P5'}$ and $^{3}J_{C4'P3'}$ to the dihedral angles β and ϵ.

to the large number of scalar coupling constants obtained (Tables 4 and 5, Supporting Information) and due to the additional use of NOE distance information, the allowed dihedral angle ranges could be restricted to relatively distinct regions. The final set of distance constraints included 184 intranucleotide constraints, 80 sequential constraints, 16 long-range constraints, and 16 hydrogen-bonding constraints. A total of 129 angle restraints were obtained from the local conformational analysis and 30 angle constraints from the phosphorus chemical shifts (Table 6, Supporting Information). The total number of constraints, 455, corresponds to an average of 24 constraints per nucleotide residue.

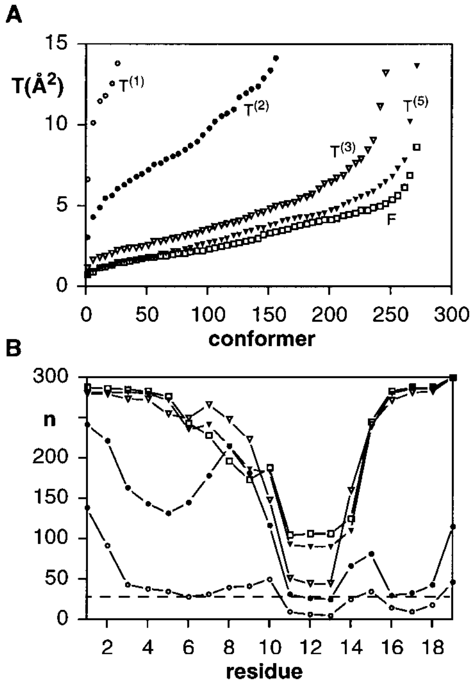

FIGURE 6: (A) Distribution of the DIANA target function values, T, among the 300 calculated conformers. $T^{(1)}$, $T^{(2)}$, $T^{(3)}$, $T^{(5)}$, and F are the target function values after the first conjugate gradient minimization of the variable target function, the second, third, and fifth minimization, which used redundant dihedral angle restraints (REDAC), and the final target function calculated with the initial set of experimentally determined angle constraints, respectively. (B) Number of locally acceptable fragments, n, for each residue after each step in the DIANA calculations using REDAC. The symbols refer to the same runs as in (A). Redundant dihedral angle restraints were only introduced if more than 30 conformers with locally acceptable residues were found (dashed line).

Structure Determination. The final structure calculations with DIANA (Güntert et al., 1991) were started with 300 randomized conformers. The course of the DIANA structure calculation is documented in Figure 6A. The first conjugate gradient minimization of the variable target function did not result in structures which could be regarded as converged due to high residual target function values (see curve $T^{(1)}$ in Figure 6A). We therefore applied the REDAC strategy (Güntert & Wüthrich, 1991) in which dihedral angle constraints are derived from locally acceptable fragments. As shown in Figure 6B, large numbers of calculated conformers with locally acceptable fragments for all residues are obtained only after several REDAC cycles. Judged on the basis of low final target function values, this strategy allowed a sufficient number of converged structures to be obtained. Residual constraint violations had small magnitudes and were few in number (Table 1). The low target function values which were obtained also indicate that there were no severe inconsistencies in the input data.

The RMSD values to the mean structure of the 15 conformers with the lowest target functions were 1.05 ± 0.36 Å for residues 2−18, 0.67 ± 0.26 Å for the helical region

Table 1: Structural Statistics of the 15 Best DIANA Conformers Representing the Solution Structure of the RNA 19-mer

parameter	DIANA[a,b]	DIANA and AMBER[a,c]
DIANA target function (Å^2)	0.99 ± 0.15 (0.72−1.20)	
upper limit violations		
no. >0.2 Å	2.5 ± 1.1 (1−4)	2.3 ± 1.6 (0−5)
sum of violations (Å)	4.2 ± 0.3 (3.7−4.9)	5.0 ± 0.5 (4.1−5.6)
max violation (Å)	0.32 ± 0.08 (0.20−0.46)	0.32 ± 0.09 (0.19−0.47)
lower limit violations		
no. >0.2 Å	0.1 ± 0.2 (0−1)	0.0 ± 0.0 (0−0)
sum of violations (Å)	0.9 ± 0.2 (0.7−1.4)	0.06 ± 0.04 (0.00−0.12)
max violation (Å)	0.12 ± 0.03 (0.11−0.23)	0.05 ± 0.03 (0.00−0.12)
dihedral angle violations		
no. >5°	0.3 ± 0.6 (0−2)	1.1 ± 1.3 (0−4)
sum of violations (deg)	22.0 ± 6.2 (13.6−31.4)	46.3 ± 9.7 (31.3−65.7)
max violation (deg)	3.9 ± 1.2 (2.1−5.7)	5.9 ± 1.4 (4.3−8.7)
AMBER energy (kcal/mol)	15 ± 36 (−62 to 92)	−694 ± 12 (−715 to −679)
RMSD values to mean structure		
residues 2−18		
backbone (Å)	0.97 ± 0.39 (0.45−2.15)	0.95 ± 0.38 (0.47−2.09)
all heavy atoms (Å)	1.05 ± 0.36 (0.53−2.03)	1.03 ± 0.34 (0.58−1.95)
helix (residues 2−7, 13−18)		
backbone (Å)	0.74 ± 0.27 (0.34−1.28)	0.68 ± 0.26 (0.33−1.23)
all heavy atoms (Å)	0.67 ± 0.26 (0.33−1.18)	0.61 ± 0.24 (0.29−1.11)
loop (residues 7−13)		
backbone (Å)	0.75 ± 0.20 (0.45−1.17)	0.78 ± 0.20 (0.44−1.10)
all heavy atoms (Å)	0.99 ± 0.26 (0.59−1.41)	1.05 ± 0.25 (0.65−1.41)

[a] The numbers are given as average value ± standard deviation. The minimum and maximum values for the 15 conformers are given in parentheses. [b] Conformers before restrained energy minimization. [c] Conformers after restrained energy minimization with AMBER.

(residues 2−7, 13−18), and 0.99 ± 0.26 Å for the loop region (residues 7−13) calculated over all heavy atoms (Table 1). After restrained energy minimization with AMBER, the mean energy of the 15 DIANA conformers was reduced by 709 kcal/mol, and the number and sum of the violations were quite constant. The mean pairwise RMSD values between the corresponding structures before and after energy minimization were 0.56 ± 0.07Å for the heavy atoms of residues 2−18. These are relatively small changes compared to the RMSDs observed between the different structures. To determine the influence of the electrostatic interactions on the restrained energy minimization, the same minimization protocol was repeated with the distance-dependent dielectric constant set to an arbitrarily high value ($\epsilon = 1000r$), thereby scaling the electrostatic interactions so that they become negligible. With this approach the mean energy of the conformers was reduced slightly less, by 615 kcal/mol. The mean pairwise RMSD values did not change, and the mean pairwise RMSD values between the corresponding structures before and after energy minimization were 0.50 ± 0.04 Å for the heavy atoms of residues 2−18. These results indicate that the inclusion of the electrostatic interactions did not lead to major changes in the structures.

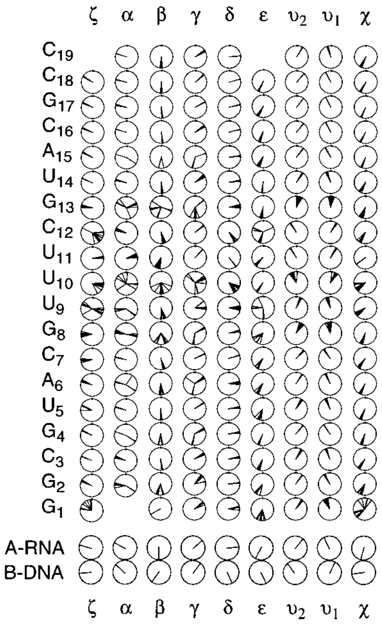

FIGURE 7: Torsion angles in the 15 final structures. Dial plots for each torsion angle in the structure are shown. Each line represents the torsion angle of one of the 15 structures. For comparison, torsion angles typical for A- and B-form helices are shown.

Structure of the 19-mer Stem Region. A superposition of the helix region (residues 2−7 and 13−18) of the RNA 19-mer is shown as a stereoview in Figure 8A. Although residues 1 and 19 showed reasonably well restricted dihedral angles (Figure 7), these residues showed the typical fraying observed for base pairs at the ends of helical regions and have therefore been omitted from Figure 8A. Typical A-form characteristics such as the deep major groove can be observed. All nucleotides of the helix region are in C3′-endo conformation with the glycosidic angles being in the anti range. Helical parameters for base pair steps have been determined with the program rna from Babcock et al. (1993) and are shown in Table 2. The helix parameters essentially agree with an A-form helical conformation being adopted by the stem nucleotides. The helix has 11.0 base pairs per turn on average, close to the 10.9 for A-form RNA. The rise and slide values are also close to those expected for A-form RNA. The roll and tilt values show larger deviations between different base pair steps as well as from the ideal A-form. The larger scattering of the values between individual structures suggests that these parameters are less well defined by the applied constraint set. In Figure 7 the torsion angles in the 15 conformers are shown. Although these are local parameters, they clearly show the characteristics of an A-form helix. Most stem nucleotides adopt a

Table 2: Helical Parameters for Base Steps in the Helix Region of the 19-mer[a] (Residues 2−7 and 13−18)

base step	helical twist (deg)	rise (Å)	slide (deg)	roll (deg)	tilt (deg)
G2−C18/C3−G17	32.8 ± 2.8	3.1 ± 0.1	−1.0 ± 0.2	12.1 ± 2.1	1.8 ± 0.9
C3−G17/G4−C16	31.1 ± 0.9	3.1 ± 0.1	−1.1 ± 0.2	17.7 ± 5.0	−0.3 ± 1.4
G4−C16/U5−A15	35.1 ± 1.3	3.1 ± 0.1	−1.2 ± 0.2	5.6 ± 2.4	−3.1 ± 1.0
U5−A15/A6−U14	30.6 ± 1.4	2.8 ± 0.1	−1.4 ± 0.1	12.9 ± 5.4	−2.9 ± 2.2
A6−U14/C7−G13	33.1 ± 2.9	3.1 ± 0.1	−0.7 ± 0.1	−2.2 ± 2.6	7.4 ± 1.3
average	32.5 ± 1.8	3.0 ± 0.1	−1.1 ± 0.3	9.2 ± 7.6	0.6 ± 4.3
A-form	32.7	2.8	−1.5	−0.4	13.0

[a] The parameters (mean ± standard deviation) were calculated using the program rna (Babcock et al., 1993). The parameters are given as described by the EMBO guidelines (Dickerson, 1989). Standard A-form parameters were taken from Wu and Turner (1996).

rather small torsion angle range in all structures. For some residues, e.g., G4, A6, and A15, for which the γ torsion angle could not be restricted to the +sc region using local conformational analysis, γ torsion angles in the ap range could also be found to fulfill all the experimental constraints. For these structures α is found to be in the +ac rather than the typical −sc region, which means that the α and γ angles are clearly correlated in the stem region.

Loop Region. A superposition of residues 7−13 of the 15 energy-minimized conformers is shown as a stereoview in Figure 8B, C. Due to the observation of some broad lines as compared to resonances in the stem, which are probably due to conformational exchange processes with lifetimes of microseconds to milliseconds (Jardetzky & Roberts, 1981), the conformation determined for the loop region has to be regarded as an average conformation. All glycosidic angles in the loop region are in the anti range, but whereas values around −130° are found for residues 9−11, the χ angle found for all other residues is around −165°, which is typical for an A-form conformation (see Figure 7). Nucleotides U10 to C12 adopt C2′-endo ribose puckers, which is fully consistent with the observed $^3J_{\mathrm{HH}}$ coupling constants (Table 4, Supporting Information). Nucleotides G8 and U9 are found in the C3′-endo conformation in the final structures although the $^3J_{\mathrm{HH}}$ coupling constants indicate that an equilibrium including a minor population of C2′-endo conformers cannot be excluded for this more flexible structural region.

The backbone of the loop shows an overall S-form shape, as can best be seen from the top view of the loop in Figure 8C. At the base of the loop next to the helical stem, bases G8 and C12 do not form a Watson−Crick base pair (Figure 8B) but rather point in the direction of the minor and major grooves, respectively. G8O6 was found to be able to form a hydrogen bond to G13H22 with a hydrogen bond distance between hydrogen and acceptor of 1.7−1.9 Å and a hydrogen−donor−acceptor angle of 1.3−14.8°. A further hydrogen bond between HO2′ of C7 and O4′ of G8 is found in about half of the structures. The base of U11 is pointing to the backbone above C7 and is in stacking distance to the C7 base in many structures (see Figures 8C and 9A). The base of U10 points in the same direction as G8 and is in stacking distance to the base of G8 in about half of the structures (see Figures 8C and 9B). Only one of the stacking interactions in the loop, G8-U10 or C7-U11, is found in the different structures, which suggests that two interconverting conformations with alternate stacking interactions are possible. This requires only moderate changes in the backbone conformation of the loop (Figures 8C and 9). The most exposed bases are U9 and C12. The base of U9 showed only one NOE to the rest of the loop and has an undefined, probably flexible conformation. The position of the base of C12 is better defined and is apparently stabilized by a hydrogen bond between O2 and the HO2′ of the same residue (Figures 8C and 9).

DISCUSSION AND CONCLUSIONS

As has been observed by NMR for several hairpin loop motifs, e.g., the 5′-CUUG-3′ tetraloop (Aboul-ela et al., 1994), the 5′-CGGUUCG-3′ motif (Sich et al., 1996), and the 5′-CGUUUCG-3′ motif studied here, there is a propensity in solution to form duplexes containing bulges with unusual base pairs. Furthermore, in X-ray crystallography it is often observed that hairpin loop motifs crystallize as duplex structures (Holbrook et al., 1991; Lietzke et al., 1996; Grüne et al., 1996a). Several studies found in the literature address this topic: e.g., Aboul-ela et al. (1994) have described methods to distinguish monomer and dimer forms of the tetraloop sequence CUUG via ^{15}N-filtered NOE experiments. This tetraloop sequence is a good example in which either hairpin loop or duplex conformations exist in solution depending on the solution conditions. We have also shown that the 5′-GUU-3′ triloop motif with a stem length of four nucleotides forms a duplex with three unusual base pairs at concentrations used for NMR spectroscopy, and alternative NMR methods to verify monomer or duplex formation by ^{15}N-labeled RNA molecules have been proposed (Sich et al., 1996). For the 5′-CGUUUCG-3′ loop motif, the rapid interconversion of monomeric and dimeric forms of the 11-mer might be related to loop−loop interactions such as those observed in “kissing complexes” (Marino et al., 1995a) since three consecutive UU base pairs are present in the duplex form (unpublished results). The structure of the UUU duplex for the 11-mer will be reported elsewhere. Our initial motivation for investigating longer stems was the expectation that longer stems would lead to the ability to kinetically trap the monomeric stem−loop in a sufficiently stable form by thermal quenching. Given that the same loop motif and flanking base pairs were used throughout and that a pentaloop seems to be formed in all cases (Figure 1), the observation that longer stems led to decreased equilibrium concentrations of duplexes was unanticipated but would be consistent with positive cooperative effects in the formation of longer helices. In the case of the present 5′-CGUUUCG-3′ loop motif, we have been able to obtain the 19-mer purely as a monomeric stem−loop species in solution under NMR conditions by increasing the stem length.

Two of the aims of the present study were (a) the determination of the structure of the 5′ -CGUUUCG-3′ loop motif by applying heteronuclear NMR techniques to obtain as many constraints as possible and (b) the evaluation of local conformational analysis, torsion angle distance geometry, and restrained energy minimization as tools for structure determination of RNA molecules. To obtain as many scalar coupling constants as possible, a method to determine both $^3J_{C4'P}$ coupling constants from a set of spin-echo difference spectra (Vuister et al., 1993) and to assign them to the torsion angles β and ϵ by the use of a simple 3D HCP experiment (Heus et al., 1994) was established. Compared to Legault et al. (1995) this method provides better restraint ranges for the two $^3J_{C4'P}$ coupling constants as well as the direct possibility to use the coupling in the restriction of specific torsion angles, β and ϵ, respectively.

For structure determination, the combined use of scalar couplings and NOEs in local conformational analysis has been shown to provide a large number of dihedral angle restraints. These, together with NOE-derived distance constraints, provided input data for distance geometry employing the program DIANA (Güntert et al., 1991), which utilizes a variable target function algorithm (Braun & Gō, 1985) and works in dihedral angle space, with the advantage that the covalent geometry is preserved during the entire calculation. For DIANA calculations, a simple conjugate gradient minimization of the variable target function was not sufficient to obtain structures of the 19-mer RNA molecule which could be regarded as converged structures, even when starting with a relatively large pool of 300 random conformers. Application of the REDAC strategy (Güntert & Wüthrich, 1991) did lead to structures with low target function values and therefore good agreement with the experimental constraints. The problem of convergence in the calculation of nucleic acid structures has recently been addressed by Stein et al. (1997). By using molecular dynamics in torsion angle space, they achieved dramatically increased convergence for DNA, whereas the use of Cartesian molecular dynamics and metric−matrix distance geometry protocols were problematic. The success of the REDAC strategy compared to a simple conjugate gradient minimization can be rationalized because, at low target levels in a DIANA calculation, multiple different local conformations may be found, some of which may be incompatible with the long-range constraints taken into account at higher minimization levels (Güntert & Wüthrich, 1991). Similarly to β strands in a protein, cross-strand constraints in oligonucleotides will have major influences on the local conformation of the opposite strand. Another reason for the success of the REDAC strategy may be related to the higher degree of freedom in torsion angle space of a nucleic acid compared to a protein. Whereas in a protein two torsion angles are sufficient to describe the backbone, assuming the peptidic bond to be in a trans conformation, in nucleic acids six torsion angles are involved, two of which (α, ζ) are very poorly constrained by experimental data. Minimization at low target levels is therefore much more likely to lead to conformations which do not fulfill the constraints at high target levels. The higher dimensionality encountered for oligonucleotides is also a likely explanation for the need for several cycles of REDAC, especially in finding loop conformations which fulfill all constraints (Figure 6). These considerations are supported by the observation that the same global conformation can be found for different combinations of torsion angles as can be seen from the dial plots in Figure 7; e.g., for residue U4 two different combinations of α and γ torsion angles can fulfill the experimental constraints. The precision of the structures obtained in the present study is among the better available NMR structures of RNA molecules at present (see RMSDs in Table 1 and Figure 8). However, these structures also reflect the local nature of most of the NMR constraints that can be obtained for oligonucleotides; i.e., despite reasonable local conformations, the structures tend to diverge over longer distances (Figure 8). Nonetheless, the present results indicate that torsion angle distance geometry together with the REDAC strategy is a viable method to establish RNA structures with precisions comparable to results achieved with other structural computation strategies.

NMR resonances with increased line widths, probably arising from conformational exchange processes with lifetimes of microseconds to milliseconds (Jardetzky & Roberts, 1981), are a commonly occurring feature of RNA structures investigated by NMR. Varani et al. (1989) interpreted the observed broad lines with a slow "breathing" mode of the whole internal loop which they studied. Wu and Turner (1996) found broadened hydrogen resonances for ribose rings at the mismatch−stem junction of an imino hydrogen bonded tandem GA mismatch. Broad resonance lines were also observed for hairpin loop motifs such as the CUUG tetraloop (Jucker & Pardi, 1995) at the U7 to G9 residues located at the 3′ end of the loop at the stem−loop boundary or in a six-nucleotide RNA hairpin loop (Fountain et al., 1996). In the 5′-CGUUUCG-3′ loop motif studied here, broadening was observed for some of the carbon resonances at the stem−loop boundary, with a more pronounced effect at the 3′ end of the loop. These broad resonances are found predominantly in the ribose/backbone region whereas the base resonances, except for a slightly broadened C8 resonance of G8, show quite uniform carbon line widths. This suggests that two or more slow exchanging species differing mainly in the backbone conformation near residues C12 and G13 exist. Consequently, the present structure is less well defined in this region. A variety of different torsion angles are found for backbone angles of C12 and G13 (Figure 7), but there are no clear correlations between different backbone angles in the presently obtained structures. It is likely that the observed effects are connected with equilibria between C2′-endo and C3′-endo puckering of the ribose rings and that attempts to further interpret the NMR data might have to deal with structural ensembles that explicitly include species with different ribose puckering.

Structures of related loop motifs such as 5′-UUUCUGA-3′ (Puglisi et al., 1990) or 5′-GCUUUGC-3′ (Davis et al., 1993) were obtained by the use of hydrogen and phosphorus NMR and provided medium resolution structures. In a recent study of the E-domain fragment of *E. coli* 5S RNA (Grüne et al., 1996b) with the loop motif 5′-GGUCUCC-3′, the imino hydrogen and amino hydrogens of the residues directly adjacent to the UCU loop as well as imino−amino NOEs were observed, indicating the formation of a Watson−Crick GC base pair. The striking difference between these loop motifs and the loop motif investigated in the present work is that the former motifs are real triloops closed by U-G, C-G, or G-C base pairs, respectively, whereas the structure presented here is a pentaloop. This serves to emphasize the context dependence of RNA structures. For example, the structures of tandem GA mismatches depend on whether the adjacent base pair is G-C or C-G (SantaLucia & Turner, 1993; Wu & Turner, 1996). As has been shown for tetraloops (Tuerk et al., 1988), the closing base pair is very important for the stability of the hairpin structure; e.g., the

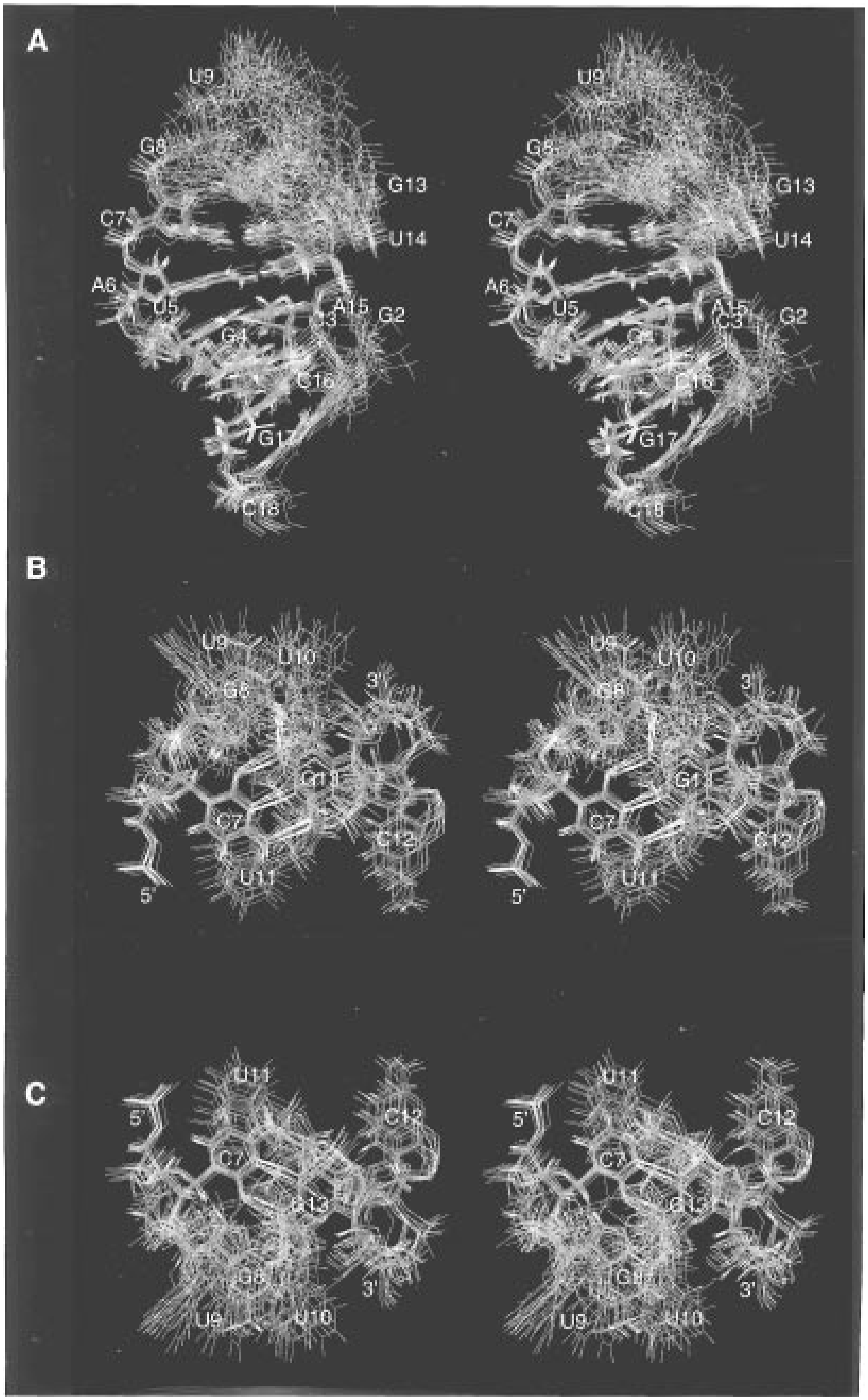

FIGURE 8: Stereoview of the superposition of the 15 final structures. (A) Residues G2−C7 and G13−C18 were fitted over all heavy atoms to the mean structure. (B, C) C7−G13, comprising the loop motif of the 19-mer. Heavy atoms of residues C7, G8 and C12, G13 were fitted to the mean structure. (B) View of the loop looking from the helix axis. (C) Same as (B) rotated by 180° around the *x*-axis. Hydrogen bonds observed in the loop are indicated by yellow lines.

5′-UUCG-3′ tetraloop preferentially closes with a C-G rather than G-C base pair (Woese et al., 1990). The present and previous results (Davis et al., 1993) would seem to indicate that the UUU triloop can apparently be closed by a pyrimidine−purine base pair but not by a G-C base pair. However, since the related UCU loop can apparently be

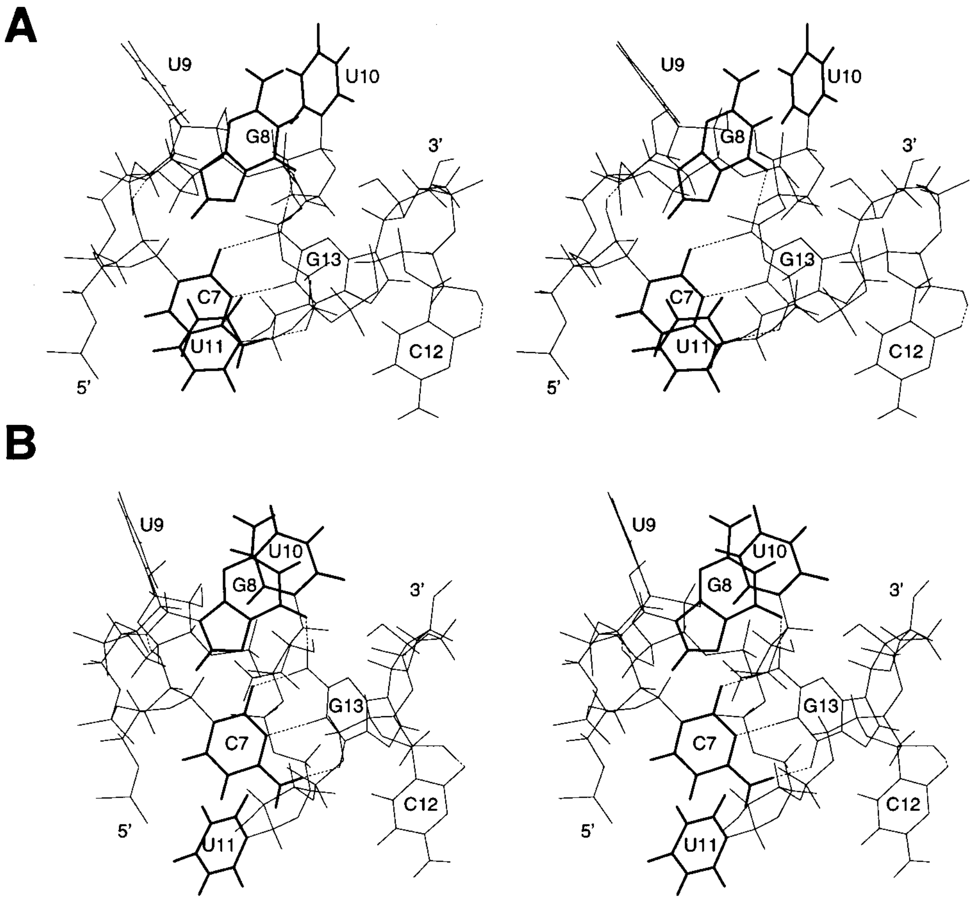

FIGURE 9: Stereoview of the loop region C7−G13 of the 19-mer looking from the helix axis. Two representative structures are shown: (A) structure with stacking interaction between the bases of C7 and U11; (B) structure with stacking interaction between the bases of G8 and U10. The bases of residues C7, G8, U10, and U11 are marked by thicker lines. Observed hydrogen bonds are indicated by dashed lines.

closed by a G-C base pair in the 5′-GGUCUCC-3′ motif (Grüne et al., 1996b), different stacking energies (G on C versus C on G) as well as different steric requirements of the closing base pair may contribute to the difference observed for the 5′-CGUUUCG-3′ motif. It is known that the free energy of formation of a CG/GC base step is approximately −3.2 kcal/mol, whereas GC/CG and GG/CC base steps have free energies of formation of −5 kcal/mol (Saenger, 1984), a difference which could contribute to existence of a pentaloop for the 5′-CGUUUCG-3′ motif. Additionally, the G8O6−G13H22 hydrogen bond observed in this study can only be formed in the 5′-CGUUUCG-3′ motif because of the position of the G amino hydrogen bond donor.

Although the UUU loop motif occurs quite frequently in 16S-like rRNAs (Wolters, 1992), the reasons for this remain unclear. A possible explanation would be that these kinds of loops provide favorable interaction sites for RNA/RNA or RNA/protein interactions. This could explain why they often occur in 16S-like rRNA variable hairpins (Wolters, 1992). The hairpin loop at position 83 (*E. coli* numbering) occurs to 45% as CUUG and to 36% as UUCG tetraloops (Woese et al., 1990) but is sometimes substituted by a UUU loop. For both of these tetraloop structures, one of the U bases in the loop does not show specific contacts within the loop motif but may provide RNA/RNA or RNA/protein interaction sites (Jucker & Pardi, 1995; Varani et al., 1991). Given that the 5′-CGUUUCG-3′ motif is the most common UUU loop in eukaryotic 18S RNA, that in eukaryotic 18S rRNA it is associated with stems longer than four base pairs, that two of the bases (U9 and C12) in the pentaloop are highly exposed and show only minimal interactions within the loop structure, and that two alternate stacking arrangements (G8-U10 or C7-U11) are apparently possible, this loop might be an example of a structurally more complex interaction site.

ACKNOWLEDGMENT

We thank R. Lamprecht and A. Figuth for help with the preparation of labeled nucleotides, H.-J. Leppert for extending the VNMR−PROSA interface, M. Semm for the modification of MOLMOL for the preparation of torsion angle plots, Dr. R. Glaser (ETH−Zürich) for providing a preliminary version of his new spectral analysis program SPSCAN which was used for the extraction of scalar coupling constants from E.COSY patterns, Dr. V. Soskic for establishing production of isotope-labeled RNA in our laboratory, and Dr. M. Grüne for help with the acquisition of some experiments. Collaboration with P. Güntert, M. Billeter, and K. Wüthrich, ETH−Zürich, in the development of software for local conformational analysis of oligonucleotides (to be published) is gratefully acknowledged. The availability of the programs RNAfold (P. Schuster, University of Vienna) and rna (M. S. Babcock, University of New Jersey) is gratefully acknowledged.

SUPPORTING INFORMATION AVAILABLE

Six tables showing (1) NMR acquisition and processing parameters of all acquired experiments, (2) proton chemical shifts of the 19-mer, (3) heteronuclear chemical shifts of the 19-mer, (4) proton−proton scalar coupling constants, (5) proton−phosphorus and carbon−phosphorus scalar coupling constants, and (6) dihedral angle restraints obtained by local conformational analysis (8 pages). Ordering information is given on any current masthead page.

REFERENCES

Aboul-ela, F., Karn, J., & Varani, G. (1995) *J. Mol. Biol. 253*, 313−332.

Aboul-ela, F., Nikonowicz, E. P., & Pardi, A. (1994) *FEBS Lett. 347*, 261−264.

Allain, F. H. T., & Varani, G. (1995) *J. Mol. Biol. 250*, 333−353.

Allain, F. H. T., Gubser, C. C., Howe, P. W. A., Nagai, K., Neuhaus, D., & Varani, G. (1996) *Nature 380*, 646−650.

Altona, C. (1982) *Recl. Trav. Chim. Pays-Bas 101*, 413−433.

Altona, C., & Sundaralingam, M. (1973) *J. Am. Chem. Soc. 95*, 2333−2344.

Babcock, M. S., Pednault, E. P. D., & Olson, W. K. (1993) *J. Biomol. Struct. Dyn. 11*, 597−627.

Bartels, C., Xia, T. H., Billeter, M., Güntert, P., & Wüthrich, K. (1995) *J. Biomol. NMR 6*, 1−10.

Batey, R. T., Inada, M., Kujawinski, E., Puglisi, J. D., & Williamson, J. R. (1992) *Nucleic Acids Res. 20*, 4515−4523.

Bax, A., Clore, G. M., Driscoll, P. C., Gronenborn, A. M., Ikura, M., & Kay, L. E. (1990) *J. Magn. Reson. 87*, 620−627.

Bodenhausen, G., & Ruben, D. J. (1980) *Chem. Phys. Lett. 69*, 185−189.

Braun, W., & Gō, N. (1985) *J. Mol. Biol. 186*, 611−626.

Cate, J. H., Gooding, A. R., Podell, E., Zhou, K., Golden, B. L., Kundrot, C. E., Cech, T. R., & Doudna, J. A. (1996) *Science 273*, 1678−1685.

Cheong, C., Varani, G., & Tinoco, I., Jr. (1990) *Nature 346*, 680−682.

Clore, G. M., Bax, A., Driscoll, P. C., Wingfield, P. T., & Gronenborn, A. M. (1990) *Biochemistry 29*, 8172−8184.

Colvin, R. A., White, S. W., Garcia-Blanco, M. A., & Hoffman, D. W. (1993) *Biochemistry 32*, 1105−1112.

Cornell, W. D., Cieplak, P., Bayly, C. I., Gould, I. R., Merz, K. M., Ferguson, D. M., Spellmeyer, D. C., Fox, T., Caldwell, J. W., & Kollman, P. A. (1995) *J. Am. Chem. Soc. 117*, 5179−5197.

Davis, P. W., Thurmes, W., & Tinoco, I., Jr. (1993) *Nucleic Acids Res. 21*, 537−545.

Dickerson, R. E. (1989) *Nucleic Acids Res. 17*, 1797−1803.

Dieckmann, T., & Feigon, J. (1994) *Curr. Opin. Struct. Biol. 4*, 745−749.

Feigon, J., Dieckmann, T., & Smith, F. W. (1996) *Chem. Biol. 3*, 611−617.

Fesik, S. W., Eaton, H. L., Olejniczak, E. T., & Zuiderweg, E. R. P. (1990) *J. Am. Chem. Soc. 112*, 886−888.

Fountain, M. A., Serra, M. J., Krugh, T. R., & Turner, D. H. (1996) *Biochemistry 35*, 6539−6548.

Gorenstein, D. G. (1984) *Phosphorus-31 NMR: Principles and Applications*, Academic Press, New York.

Gregorian, R. S., Jr., & Crothers, D. M. (1995) *J. Mol. Biol. 248*, 968−984.

Griesinger, C., & Eggenberger, U. (1992) *J. Magn. Reson. 97*, 426−434.

Grüne, M., Fürste, J. P., Klussmann, S., Erdmann, V. A., & Brown, L. R. (1996a) *Nucleic Acids Res. 24*, 2592−2596.

Grüne, M., Görlach, M., Soskic, V., Klussmann, S., Bald, R., Fürste, J. P., Erdmann, V. A., & Brown, L. R. (1996b) *FEBS Lett. 385*, 114−118.

Grzesiek, S., & Bax, A. (1993) *J. Am. Chem. Soc. 115*, 12593−12594.

Güntert, P., & Wüthrich, K., (1991) *J. Biomol. NMR 1*, 447−456.

Güntert, P., Braun, W., & Wüthrich, K., (1991) *J. Mol. Biol. 217*, 517−530.

Güntert, P., Dötsch, V., Wider, G., & Wüthrich, K., (1992) *J. Biomol. NMR 2*, 619−629.

Güntert, P., Berndt, K. D., & Wüthrich, K. (1993) *J. Biomol. NMR 3*, 601−606.

Heus, H. A., & Pardi, A. (1991a) *J. Am. Chem. Soc. 113*, 4360−4361.

Heus, H. A., & Pardi, A. (1991b) *Science 253*, 191−194.

Heus, H. A., Wijmenga, S. S., van de Ven, F. J. M., & Hilbers, C. W. (1994) *J. Am. Chem. Soc. 116*, 4983−4984.

Hoffman, D. W., Colvin, R. A., Garcia-Blanco, M. A., & White, S. W. (1993) *Biochemistry 32*, 1096−1104.

Holbrook, S. R. Cheong, C., Tinoco, I., Jr., & Kim, S.-H. (1991) *Nature 353*, 579−581.

Jaeger, J. A., & Tinoco, I., Jr. (1993) *Biochemistry 32*, 12522−12530.

Jardetzky, O., & Roberts, G. C. K. (1981) *NMR in Molecular Biology*, Academic Press, Inc., Orlando, FL.

Jucker, F. M., & Pardi, A. (1995) *Biochemistry 34*, 14416−14427.

Kay, L. E., Ikura, M., & Bax, A. (1990) *J. Am. Chem. Soc. 112*, 888−889.

Koradi, R., Billeter, M., & Wüthrich, K., (1996) *J. Mol. Graphics 14*, 51−55.

Kumar, A., Ernst, R. R., & Wüthrich, K., (1980) *Biochem. Biophys. Res. Commun. 95*, 1−6.

Laing, L. G., & Hall, K. B. (1996) *Biochemistry 35*, 13586−13596.

Lee, C.-H., & Sarma, R. H. (1976) *J. Am. Chem. Soc. 98*, 3541−3548.

Legault, P., Farmer, B. T., II, Mueller, L., & Pardi, A. (1994) *J. Am. Chem. Soc. 116*, 2203−2204.

Legault, P., Jucker, F. M., & Pardi, A. (1995) *FEBS Lett. 362*, 156−160.

Lietzke, S. E., Barnes, C. L., Berglund, J. A., & Kundrot, C. E. (1996) *Structure 4*, 917−930.

Lippens, G., Dhalluin, C., & Wieruszeski, J. M. (1995) *J. Biomol. NMR 5*, 327−331.

Marino, J. P., Prestegard, J. H., & Crothers, D. M. (1994a) *J. Am. Chem. Soc. 116*, 2205−2206.

Marino, J. P., Schwalbe, H., Anklin, C., Bermel, W., Crothers, D. M., & Griesinger, C. (1994b) *J. Am. Chem. Soc. 116*, 6472−6473.

Marino, J. P., Gregorian, R. S., Csankovszki, G., & Crothers, D. M. (1995a) *Science 268*, 1448−1454.

Marino, J. P., Schwalbe, H., Anklin, C., Bermel, W., Crothers, D. M., & Griesinger, C. (1995b) *J. Biomol. NMR 5*, 87−92.

Marino, J. P., Schwalbe, H., Glaser, S. J., & Griesinger, C. (1996) *J. Am. Chem. Soc. 118*, 4388−4395.

Milligan, J. F., Groebe, D. R., Witherell, G. W., & Uhlenbeck, O. C., (1987) *Nucleic Acids Res. 15*, 8783−8798.

Mirmira, S. R., & Tinoco, I., Jr. (1996) *Biochemistry 35*, 7664−7674.

Moore, P. B. (1993) *Curr. Opin. Struct. Biol. 3*, 340−344.

Moore, P. B. (1995) *Acc. Chem. Res. 28*, 251−256.

Mooren, M. M. W., Wijmenga, S. S., van der Marel, G. A., van Boom, J. H., & Hilbers, C. W. (1994) *Nucleic Acids Res. 22*, 2658−2666.

Nikonowicz, E. P., & Pardi, A. (1993) *J. Mol. Biol. 232*, 1141−1156.

Nikonowicz, E. P., Sirr, A., Legault, P., Jucker, F. M., Baer, L. M., & Pardi, A. (1992) *Nucleic Acids Res. 20*, 4507−4513.

Norwood, T. J., Boyd, J., Heritage, J. E., Soffe, N., & Campbell, I. D. (1990) *J. Magn. Reson. 87*, 488−501.

Olsen, H. B., Ludvigsen, S., & Sørensen, O. W. (1993) *J. Magn. Reson. A105*, 321−322.

Orita, M., Nishikawa, F., Shimayama, T., Taira, K., Endo, Y., & Nishikawa, S. (1993) *Nucleic Acids Res. 21*, 5670−5678.

Pardi, A. (1995) *Methods Enzymol. 261*, 350−380.

Pardi, A., & Nikonowicz, E. P. (1992) *J. Am. Chem. Soc. 114*, 9202−9203.

Pearlman, D. A., Case, D. A., Caldwell, J. W., Ross, W. S., Cheatham, T. E., III, Ferguson, D. M., G. L. Seibel, U. C. Singh, P. K. Weiner, & Kollman, P. A. (1995) *AMBER 4.1*, University of California, San Francisco.

Pingoud, A., Fliess, A., & Pingoud, V. (1989) in *HPLC of Macromolecules* (Oliver, R. W. A., Ed.) pp 183−208, IRL Press at Oxford University Press, Oxford, U.K.

Plavec, J., & Chattopadhyaya, J. (1995) *Tetrahedron Lett. 36*, 1949−1952.

Pley, H. W., Flaherty, K. M., & McKay, D. B. (1994a) *Nature 372*, 111−113.

Pley, H. W., Flaherty, K. M., & McKay, D. B. (1994b) *Nature 372*, 68−74.

Puglisi, J. D., & Tinoco, I., Jr. (1989) *Methods Enzymol. 180*, 304−325.

Puglisi, J. D., Wyatt, J. R., & Tinoco, I., Jr. (1990) *Biochemistry 29*, 4215−4226.

Ramachandran, R., Sich, C., Grüne, M., Soskic, V., & Brown, L. R. (1996) *J. Biomol. NMR 7*, 251−255.

Ramachandran, R., Sich, C., Ohlenschläger, O., & Brown, L. R. (1997) *J. Magn. Reson. 124*, 210−213.

Saenger, W. (1984) *Principles of Nucleic Acid Structure*, Springer-Verlag, New York.

SantaLucia, J., Jr., & Turner, D. H. (1993) *Biochemistry 32*, 12612−12623.

Santoro, J., & King, G. C. (1992) *J. Magn. Reson. 97*, 202−207.

Schmieder, P., Ippel, J. H., van den Elst, H., van der Marel, G. A., van Boom, J. H., Altona, C., & Kessler, H. (1992) *Nucleic Acids Res. 20*, 4747−4751.

Schmitz, U., & James, T. L. (1995) *Methods Enzymol. 261*, 3−44.

Schwalbe, H., Marino, J. P., King, G. C., Wechselberger, R., Bermel, W., & Griesinger, C. (1994) *J. Biomol. NMR 4*, 631−644.

Schwalbe, H., Marino, J. P., Glaser, S. J., & Griesinger, C. (1995) *J. Am. Chem. Soc. 117*, 7251−7252.

Scott, W. G., Murray, J. B., Arnold, J. R. P., Stoddard, B. L., & Klug, A. (1996) *Science 274*, 2065−2069.

Shen, L. X., Cai, Z., & Tinoco, I., Jr. (1995) *FASEB J. 9*, 1023−1033.

Sich, C., Flemming, J., Ramachandran, R., & Brown, L. R. (1996) *J. Magn. Reson. B112*, 275−281.

Sklenar, V., Peterson, R. D., Rejante, M. R., & Feigon, J. (1993) *J. Biomol. NMR 3*, 721−727.

Stein, E. G., Rice, L. M., & Brünger, A. T. (1997) *J. Magn. Reson. 124*, 154−164.

Szewczak, A. A., Moore, P. B., Chang, Y. L., & Wool, I. G. (1993) *Proc. Natl. Acad. Sci. U.S.A. 90*, 9581−9585.

Tate, S., Ono, A., & Kainosho, M. (1995) *J. Magn. Reson. B106*, 89−91.

Tuerk, C., Gauss, P., Thermes, C., Groebe, D. R., Gayle, M., Guild, N., Stormo, G., D'Aubenton-Carafa, Y., Uhlenbeck, O. C., Tinoco, I., Jr., Brody, E. N., & Gold, L. (1988) *Proc. Natl. Acad. Sci. U.S.A. 85*, 1364−1368.

Uhlenbeck, O. C. (1990) *Nature 346*, 613−614.

Varani, G., & Tinoco, I., Jr. (1991) *Q. Rev. Biophys. 24*, 479−532.

Varani, G., Wimberley, B., & Tinoco, I., Jr. (1989) *Biochemistry 28*, 7760−7772.

Varani, G., Cheong, C., & Tinoco, I., Jr. (1991) *Biochemistry 30*, 3280−3289.

Varani, G., Aboul-ela, F., & Allain, F. H.-T. (1996) *Prog. NMR Spectrosc. 29*, 51−127.

Vuister, G. W., & Bax, A. (1992) *J. Magn. Reson. 98*, 428−435.

Vuister, G. W., Wang, A. C., & Bax, A. (1993) *J. Am. Chem. Soc. 115*, 5334−5335.

Woese, C. R., Winkler, S., & Gutell, R. R. (1990) *Proc. Natl. Acad. Sci. U.S.A. 87*, 8467−8471.

Wolters, J. (1992) *Nucleic Acids Res. 20*, 1843−1850.

Wu, M., & Turner, D. H. (1996) *Biochemistry 35*, 9677−9689.

Wüthrich, K., (1986) *NMR of Proteins and Nucleic Acids*, John Wiley & Sons, New York.

Wyatt, J. R., Chastain, M., & Puglisi, J. D. (1991) *Biotechniques 11*, 764−769.

Xia, T. (1992) Ph.D. Thesis, ETH−Zürich.

BI971207G